Eur J Drug Metab Pharmacokinet (2016) 41:267–280
DOI 10.1007/s13318-015-0253-x

ORIGINAL PAPER

Physiologically based modeling of the pharmacokinetics of acetaminophen and its major metabolites in humans using a Bayesian population approach

Todd J. Zurlinden · Brad Reisfeld

Received: 17 September 2014 / Accepted: 9 January 2015 / Published online: 31 January 2015
© Springer International Publishing Switzerland 2015

Abstract The principal aim of this study was to develop, validate, and demonstrate a physiologically based pharmacokinetic (PBPK) model to predict and characterize the absorption, distribution, metabolism, and excretion of acetaminophen (APAP) in humans. A PBPK model was created that included pharmacologically and toxicologically relevant tissue compartments and incorporated mechanistic descriptions of the absorption and metabolism of APAP, such as gastric emptying time, cofactor kinetics, and transporter-mediated movement of conjugated metabolites in the liver. Through the use of a hierarchical Bayesian framework, unknown model parameters were estimated using a large training set of data from human pharmacokinetic studies, resulting in parameter distributions that account for data uncertainty and inter-study variability. Predictions from the model showed good agreement to a diverse test set of data across several measures, including plasma concentrations over time, renal clearance, APAP absorption, and pharmacokinetic and exposure metrics. The utility of the model was then demonstrated through predictions of cofactor depletion, dose response of several pharmacokinetic endpoints, and the relationship between APAP biomarker levels in the plasma and those in the liver. The model addressed several limitations in previous PBPK models for APAP, and it is anticipated that it will be useful in predicting the pharmacokinetics of APAP in a number of contexts, such as extrapolating across doses, estimating internal concentrations, quantifying population variability, assessing possible impacts of drug coadministration, and, when coupled with a suitable pharmacodynamic model, predicting toxicity.

Keywords Acetaminophen · APAP · PBPK · Physiologically based pharmacokinetic modeling · Bayesian population

Key Points

- A new physiologically based pharmacokinetic model was developed to describe the absorption, distribution, metabolism and excretion of acetaminophen and its conjugated metabolites in humans
- The model included mechanistic descriptions of the absorption and metabolism of acetaminophen, a Bayesian approach to model parameterization that accounts for data uncertainty and inter-study variability, and utilization of a comprehensive set of human pharmacokinetic data for model calibration and validation
- It is anticipated that the model will be useful in applications such as dose extrapolation studies; determining the tissue-specific pharmacokinetics in susceptible, vulnerable, and health-compromised populations; estimating the internal dose based on plasma levels; and assessing toxicity through integration with appropriate pharmacodynamic models

1 Introduction

Acetaminophen (paracetamol, acetyl-para-aminophenol) (APAP) is one of the most widely used analgesic and

T. J. Zurlinden · B. Reisfeld (✉)
Department of Chemical and Biological Engineering, Colorado State University, Fort Collins, CO 80523-1370, USA
e-mail: brad.reisfeld@colostate.edu

B. Reisfeld
School of Biomedical Engineering, Colorado State University, Fort Collins, CO 80523-1370, USA

antipyretics in the world. Owing to its ubiquitous usage, potential for hepatotoxicity, and varying pharmacological effects across diverse and susceptible populations, numerous human pharmacokinetic studies have been conducted for this drug (Ameer et al. 1981; Chen et al. 1996; Chiew et al. 2010; Chan et al. 1997; Critchley et al. 1986, 2005; Esteban et al. 1996; Jensen et al. 2004; Itoh et al. 2002; Kamali 1993; Kim et al. 2011; Lau and Critchley 1994; Prescott 1980; Prescott et al. 1989; Rawlins and Henderson 1977; Shinoda et al. 2007; Tan et al. 2012; Tonoli et al. 2012; Volak et al. 2013; Yin et al. 2001; Zhu et al. 2007). To quantify the results of such studies, non-compartmental (Prescott 1980; Shinoda et al. 2007; Tan et al. 2012; Volak et al. 2013; Yin and Tomlinson 2001) and compartmental (Ameer et al. 1981; Rawlins and Henderson 1977; Clements et al. 1978; Srinivasan et al. 1994) approaches have often been employed to determine the degree of exposure following administration of the drug (such as the area under the curve, AUC) and the drug's associated pharmacokinetic (PK) parameters, such as clearance, elimination half-life, and the maximum concentration (C_{max}). Although useful and widely employed, these modeling approaches are limited in their ability to predict drug disposition in a tissue-specific manner, extrapolate across dosing scenarios, and account for an individual's unique anatomical, physiological, and biochemical features. One approach that is well suited for making such predictions, and is increasingly used in the field of pharmaceutical sciences (Peters 2012), is physiologically based pharmacokinetic (PBPK) modeling (Campbell et al. 2012; Reisfeld et al. 2007).

There are presently several PBPK models for APAP and its metabolites, each of which was developed with different aims and a distinct approach. As part of a series of PBPK models for drug disposition in children, Edgington et al. (2006) developed a PBPK model for APAP that utilized age-dependent anatomical and physiological parameter values. Results from this model showed reasonable agreement with values in the literature for several pharmacokinetic parameters, such as volume of distribution at steady state and drug half-life; however, there were significant differences between predicted and experimental values for plasma concentrations of APAP for many of the values compared. Although not physiologically based, Ben-Shachar et al. (2012) created a multi-compartmental mathematical model to predict time-course plasma concentrations of APAP, accumulation of APAP and its metabolites in the urine, and glutathione (GSH) depletion. The model trends were in rough agreement with experimental data, but because it was not physiologically based, it is anticipated that accurate model predictions beyond the conditions used for calibration would be unlikely. With the aim of predicting APAP toxicity in humans, Péry et al. (2013) coupled a PBPK and a toxicodynamic model to make predictions of APAP toxicity in humans. By utilizing in vitro data from rats and quantitative structure activity relationships to estimate model parameters, this approach could potentially reduce the need for extensive PK data from animals when developing PBPK models. Predictions from the model were in reasonable agreement with plasma PK data from rats; however, the model was not validated using human data, and since previous studies have shown that there are significant differences in phase II metabolism between rats and humans (Lin and Lu 1997), such an extrapolation is likely to be problematic. To better understand APAP-induced hepatoxicity under several physiological conditions, Navid et al. (2013) created a PBPK model that included a quantitative description of GSH kinetics and semi-empirical relationships for chronic APAP uptake. Model predictions were in good agreement with plasma PK data from both a single-dose and a multiple-dosing study. Unfortunately, model predictions of GSH levels and kinetics were not compared to experimental values, and the model equations contained no allometric scaling in the physiological parameters, limiting its utility beyond the range of data used for calibration. To better understand the kinetics of glutathione depletion and the role of ophthalmic acid and 5-oxoproline in GSH metabolism, Geenen et al. (2013) developed a PBPK model for APAP that consisted of a small number of compartments (lung, kidney, liver, and "other tissue") and a detailed mathematical specification of GSH kinetics. Model predictions were in reasonable-to-good agreement with various PK data from APAP dosing in both rats and humans. Assessing the accuracy and predictive capabilities of this model and others described previously is hampered by the lack of detail provided with respect to data and model uncertainty; it is also unclear whether the same data used to illustrate the accuracy of model predictions were the same as those used for model calibration and parameter estimation.

The focus of the present work was to develop and demonstrate a new PBPK model that addresses some of the limitations of previous approaches and provides an accurate means of predicting the ADME of APAP and its conjugated metabolites in humans. To this end, the model integrated mechanistic descriptions of the absorption and metabolism of APAP, a Bayesian approach to model parameterization that accounts for data uncertainty and inter-study variability, and utilization of a comprehensive set of human pharmacokinetic data for model calibration and validation.

2 Methods

2.1 Compiling and classifying experimental data from the literature

A comprehensive review of the literature was conducted to identify adult human pharmacokinetic studies

Table 1 Human studies with pharmacokinetic data considered for analysis

References	Route of administration	Dose	Measured biomarkers	Number of subjects (sex)	Use in model development: training (T) or test/validation (V)
Ameer et al. (1981)	Oral	650 mg	Plasma: APAP	1 (M)	V
	IV	650 mg	Plasma: APAP	1 (M)	V
Chen et al. (1996)	Oral	1,000 mg	Plasma and urine: APAP, APAP-G, APAP-S	10 (M/F)	[a]
Chiew et al. (2010)	Oral	80 mg/kg	Plasma: APAP, APAP-G, APAP-S	9 (M/F)	T
Chan et al. (1997)	Oral	20 mg/kg	Plasma: APAP, APAP-G, APAP-S	6 (M/F)	T
Critchley et al. (2005)	Oral	20 mg/kg	Plasma and urine: APAP, APAP-G, APAP-S	11 (M/F)	V
	Oral	20 mg/kg	Plasma and urine: APAP, APAP-G, APAP-S	9 (M/F)	V
Critchley et al. (1986)	Oral	1,500 mg	Urine: APAP, APAP-G, APAP-S	111 (M/F)	T
Esteban et al. (1996)	Oral	1,500 mg	Urine: APAP, APAP-G, APAP-S	71 (M/F)	V
Jensen et al. (2004)	Oral	1,000 mg	Plasma: APAP, APAP-G, APAP-S	6 (M/F)	V
Itoh et al. (2001)	Oral	1,000 mg	Plasma: APAP, APAP-G, APAP-S	5 (M)	V
Kamali (1993)	Oral	1,500 mg	Plasma: APAP, urine: APAP, APAP-G, APAP-S	10 (M/F)	V
Kim et al. (2011)	Oral	1,000 mg	Plasma: APAP, APAP-G, APAP-S	12 (M/F)	V
Lau and Critchley (1994)	Oral	20 mg/kg	Plasma and urine: APAP, APAP-G, APAP-S	6 (M/F)	T
Prescott (1980)	Oral	20 mg/kg	Plasma and urine: APAP, APAP-G, APAP-S	8 (M/F)	T
	Oral	12 mg/kg	Plasma: APAP	4 (M/F)	T
	IV	12 mg/kg	Plasma: APAP	4 (M/F)	T
Prescott (1989)	Oral	1,000 mg	Plasma: APAP, APAP-G, APAP-S	10	V
Rawlins and Henderson (1977)	Oral	500 mg	Plasma: APAP	6 (M)	V
	Oral	1,000 mg	Plasma: APAP	6 (M)	V
	Oral	2,000 mg	Plasma: APAP	6 (M)	V
	IV	1,000 mg	Plasma: APAP	6 (M)	T
Shinoda et al. (2077)	Oral	1,000 mg	Plasma: APAP, APAP-G, APAP-S	5 (M/F)	T
Tan et al. (2012)	Oral	500 mg	Plasma and urine: APAP, APAP-G	12 ([c])	T
Tonoli et al. (2012)	IV	1,000 mg	Plasma: APAP, APAP-G	2 ([c])	V
Volak et al. (2013)	Oral	325 mg	Plasma: APAP, APAP-G, APAP-S	8 (M/F)	T
Yin and Tomlinson (2001)	Oral	500	Plasma: APAP	12 (M)	V
Zhu et al. (2007)	Oral	650 mg	Plasma: APAP	10 (M)	[b]

[a] Data were not used. APAP-G measurement methodology was different from that used in other studies

[b] Data were not used. APAP was administered in combination with Tramadol

[c] Not specified

where APAP was administered in a single oral or intravenous dose. Emphasis was placed on identifying studies in which two major APAP metabolites, APAP-glucuronide (APAP-G) and APAP-sulfate (APAP-S), were quantified in addition to parent APAP. Studies were divided into a training set to be used for parameter estimation (model calibration) and a test set for verification and evaluation (model validation). A summary of the studies and their characteristics and classifications is given in Table 1.

2.2 Model description and formulation

In the following sections, we detail the model structure and the equations specifying the ADME within the model compartments.

2.2.1 Model structure and physiological parameters

As depicted in Fig. 1, the PBPK model structure developed for APAP, APAP-G, and APAP-S consisted of compart-

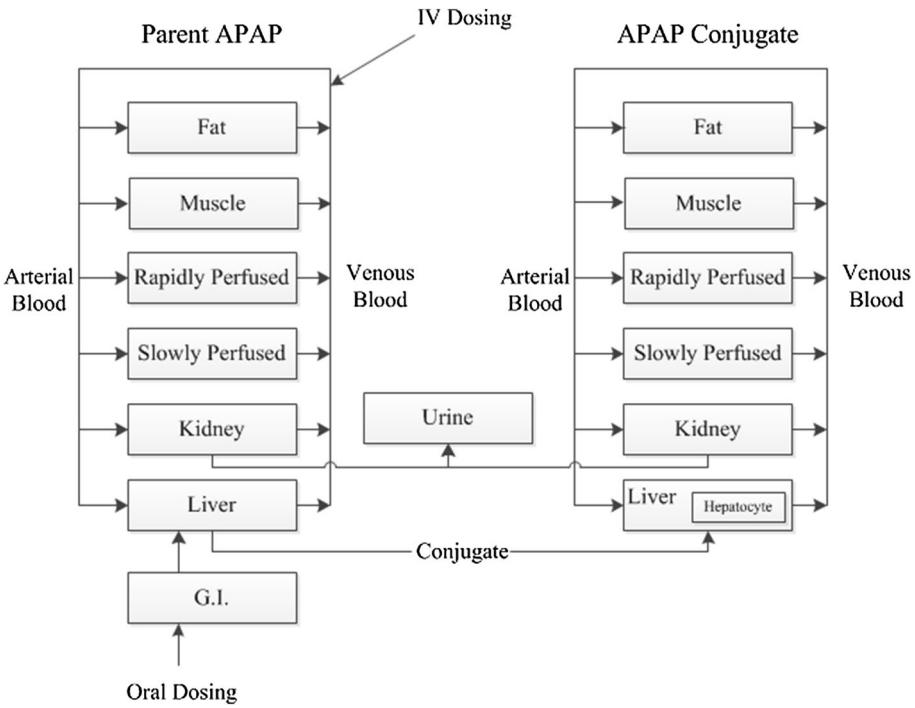

Fig. 1 PBPK model structure

ments representing fat, muscle, liver, gastrointestinal (GI), and kidney, with remaining tissues lumped (Campbell et al. 2012) into either rapidly perfused or slowly perfused compartments. All compartments were assumed to be perfusion limited (Vajjah et al. 2012). Compartmental volumes and blood flow rates (Table 2) were taken from Brown et al. (1997), and volumes and flow rates for the rapidly and slowly perfused compartments were calculated as the mean values for the lumped tissues from Brown et al. (1997).

2.2.2 *Absorption*

Several processes contribute to the absorption kinetics of APAP administered orally, including dissolution of the dose in the stomach, gastric emptying, and absorption down the length of the small intestine. To quantify these effects, the "averaged model" from Levitt (2013) was used. This relationship, representing an approximate spatially averaged solution of the diffusion-convection equation, takes the following form:

$$\begin{aligned} \frac{dA_{GI}^{APAP}}{dt} &= I(t) - \frac{dA_{abs}}{dt} \\ \frac{dA_{abs}}{dt} &= \frac{M\left[\exp\left(\frac{-t}{T_G}\right) - \exp\left(\frac{-t}{T_P}\right)\right]}{T_G - T_P} \\ M &= F_A \cdot D_{oral} \end{aligned} \quad (1)$$

Consistent with a previous convention (Reisfeld 2007), symbols indicating amounts and concentrations are given with a subscript indicating the tissue or compartment involved and a superscript indicating the chemical species. Here, A_{GI}^{APAP} is the amount of APAP in the GI

Table 2 Physiological parameters

Compartment	Value
Cardiac output	
Q_{CC}	16.2
Fat	
Q_{FC}	0.052
V_{FC}	0.21
Muscle	
Q_{MC}	0.19
V_{MC}	0.4
Liver	
Q_{LC}	0.28
V_{LC}	0.026
Kidney	
Q_{KC}	0.18
V_{KC}	0.0044
Slowly perfused	
Q_{SC}	0.14
V_{SC}	0.19
Rapidly perfused	
Q_{RC}	0.22
V_{RC}	0.077
Arterial blood	
V_{BLAC}	0.024
Venous blood	
V_{BLVC}	0.056

Cardiac output is expressed in units of L/(h-BW$^{0.75}$), while remaining tissue blood flow rates are expressed as fractions of cardiac output. Tissue volumes are expressed as L/BW$^{0.75}$

Rapidly perfused tissue comprised brain, lung, and spleen tissues, while slowly perfused consisted of bone, heart and skin (Campbell et al. 2012)

compartment. Additionally, A_{abs} is the amount of APAP absorbed into the bloodstream, t is time, $I(t)$ is the initial rate of dosing to the stomach, M is the total amount of drug available for absorption, D_{oral} is the initial APAP dose, and T_G and T_P represent time constants for gastric emptying and intestinal permeability, respectively. The fraction of APAP absorbed, F_A, has been shown to be dose-dependent at doses less than 1,000 mg (Rawlins and Henderson 1977). To account for this effect in the model, the following equation was developed:

$$F_A = \begin{cases} 0.0005 \cdot D_{oral} + 0.37, & \text{if } D_{oral} \leq 1,000\,\text{mg}, \\ 0.88 & \text{if } D_{oral} > 1,000\,\text{mg} \end{cases}. \quad (2)$$

Predictions from Eq. 2 are in good agreement with the bioavailability data from the literature (Ameer et al. 1981; Rawlins and Henderson 1977; Volak et al. 2013). For example, for a 350-mg dose, the measured and predicted values of the fraction absorbed are 0.57 (Volak et al. 2013) and 0.55, respectively, while for a 650-mg dose the values are 0.75 (Ameer et al. 1981) and 0.7, respectively.

2.2.3 Tissue distribution

Assuming passive diffusion into and out of the tissue, the rate of change of concentration within a compartment is given by the species mass balance equation

$$\frac{dA_T^j}{dt} = V_T \frac{dC_T^j}{dt} = Q_T\left(C_A^j - C_{V-T}^j\right)$$
$$C_{V-T}^j = \frac{C_T^j}{P_{T:blood}}, \quad (3)$$

where A_T^j is the amount of species j within the tissue compartment T, V_T is the volume of compartment T, C_A^j is the concentration of the chemical in the arterial blood flowing into the tissue, C_{V-T}^j is the concentration of drug flowing out of the compartment into the venous blood, and $P_{T:blood}$ is the tissue:blood partition coefficient. Values for the tissue:blood partition coefficients were determined using the method from Rodgers et al. (2006), which requires specification of several physicochemical properties of the molecule of interest. Table 3 lists the values of these parameters for APAP, APAP-G, and APAP-S, along with the calculated partition coefficients for each model compartment. Finally, because there is negligible protein binding of APAP in the blood (Naritomi et al. 2003; Gwilt et al. 1963), a blood-to-plasma concentration ratio of one was used for each species.

2.2.4 Metabolism and clearance

As depicted in Fig. 2, major routes of metabolism of APAP in the liver include glucuronidation to form APAP-G, sulfation to APAP-S, and cytochrome P450-mediated bioactivation to the glutathione-depleting species *N*-acetyl-*p*-benzoquinone imine (NAPQI) (Chan et al. 1997; Critchley et al. 1986, 2005). As shown, the phase II pathways require a cofactor for conjugation: uridine diphosphate glucuronic acid (UDPGA) for glucuronidation and 3′-phosphoadenosine-5′-phosphosulfate (PAPS) for sulfation. In humans, the percentage of APAP metabolized is roughly 54–58 % to APAP-G through UDP-glucuronosyltransferase (UGT) (Critchley et al. 1986; Prescott 1980; Forrest et al. 1982), 29–32 % to APAP-S through sulfotransferases (SULT) (Critchley et al. 1986; Prescott 1980; Forrest et al. 1982), and 4–8 % to NAPQI through cytochrome P450 isozymes (Forrest et al. 1982; Rumack 2002).

Table 3 Drug specific physiochemical properties and resulting tissue:blood partition coefficients

	APAP	APAP-G	APAP-S
Physicochemical properties (Morris and Levy 1984; Wishart et al. 2013)			
pKa_1	9.96	3.17	−2.2
pKa_2	−4.4	−3.7	−4.4
log$P$	0.91	−0.68	−1
Fraction unbound	0.82	0.92	0.46
Calculated partition coefficients			
P_{fat}	0.447	0.128	0.088
P_{muscle}	0.687	0.336	0.199
P_{kidney}	0.711	0.392	0.261
P_{liver}	0.687	0.321	0.203
P_{rapid}	0.676	0.364	0.207
P_{slow}	0.606	0.351	0.254

These processes of APAP metabolism were specified mathematically as follows. For phase I metabolism, standard Michaelis-Menten saturation kinetics were used to describe the APAP oxidation,

$$v_{cyp} = \frac{V_{M-cyp} C_{liver}^{APAP}}{K_{M-cyp}^{APAP} + C_{liver}^{APAP}}, \quad (4)$$

where v_{cyp} is the rate of APAP conversion, and V_{M-cyp} and K_{M-cyp}^{APAP} represent the Michaelis-Menten constants for APAP biotransformation through cytochrome p450 isozymes. Because the phase II conjugation pathways involve both co-substrate and substrate inhibition (Forrest et al. 1982; Mutlib et al. 2006; Nagar et al. 2006), bi-bi enzyme kinetics (Marangoni 2002) with APAP substrate inhibition were used to specify the rates of conjugation formation:

$$v_{conjugate} = \frac{V_{M-enz} C_{liver}^{APAP} \phi_{liver}^{cf}}{\left(K_{M-enz}^{APAP} + C_{liver}^{APAP} + \frac{\left(C_{liver}^{APAP}\right)^2}{K_{I-enz}}\right)\left(K_{M-enz}^{cf} + \phi_{liver}^{cf}\right)}. \quad (5)$$

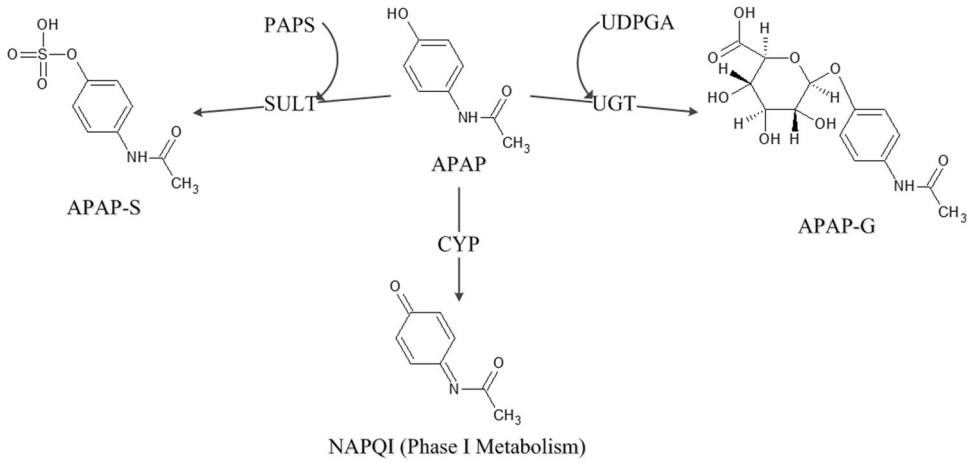

Fig. 2 Principal pathways for APAP metabolism in humans

Here, $v_{\text{conjugate}}$ is the rate of APAP conversion to conjugate; $V_{M-\text{enz}}$ is the enzyme-specific maximum rate of conversion; $K_{M-\text{enz}}^{\text{APAP}}$ and $K_{I-\text{enz}}^{\text{APAP}}$ represent the Michaelis-Menten constants and inhibition constants for APAP, respectively; $\phi_{\text{liver}}^{\text{cf}}$ is the fraction of cofactor available for reaction within the liver. As the abundance of enzyme depends on liver mass, values of the maximum rates of conversion in Eqs. 4 and 5 were computed through allometric scaling of corresponding values from the literature, $V_{MC-\text{enz}}$, by the equation $V_{M-\text{enz}} = V_{MC-\text{enz}} \cdot \text{BW}^{0.75}$, where BW is body weight.

The rates of formation and depletion of the cofactors UDPGA and PAPS influence the levels of APAP conjugates (Martin et al. 1993; Clements et al. 1984) and mediate the flux of APAP through the phase I metabolic pathway to NAPQI (Fong et al. 2011). To quantify this effect, it was assumed that the rate of cofactor depletion is equal to the rate of APAP consumption for the associated enzyme and that cofactor is regenerated once APAP concentrations in the liver are reduced. The resulting relationship for cofactor kinetics then takes the form

$$\frac{\text{d}A_{\text{liver}}^{\text{cf}}}{\text{d}t} = -v_{\text{conjugate}} + k_{\text{syn}-\text{cf}}\left(1 - \phi_{\text{liver}}^{\text{cf}}\right), \tag{6}$$

where $A_{\text{liver}}^{\text{cf}}$ is the amount of cofactor in the liver, $v_{\text{conjugate}}$ is the rate of conjugate formation, and $k_{\text{syn}\ -\ \text{cf}}$ represents the rate of synthesis of the cofactor.

In addition to cofactor kinetics, active transport of the conjugates from hepatocytes into the extracellular environment has a significant influence on APAP metabolism and clearance. Iida and coworkers (1989) demonstrated that APAP freely diffuses into hepatocytes, but once it is metabolized to either APAP-G or APAP-S, membrane transporters facilitate movement of these conjugated molecules into the greater liver parenchyma. Following their mathematical description, the rate of transport of a given conjugate, $v_{\text{mem}-\text{conj}}$, was assumed to follow saturation kinetics,

$$v_{\text{mem}}^{\text{conj}} = \frac{V_{M-\text{mem}}^{\text{conj}} C_{\text{hep}}^{\text{conj}}}{K_{M-\text{mem}}^{\text{conj}} + C_{\text{hep}}^{\text{APAP}}}, \tag{7}$$

where $V_{M-\text{mem}}^{\text{conj}}$ and $K_{M-\text{mem}}^{\text{conj}}$ are the kinetic parameters for membrane transport, and $C_{\text{hep}}^{\text{conj}}$ is the concentration of conjugate within the hepatocyte.

The final factor considered with regard to clearance of APAP and its metabolites was renal excretion to the urine, which was modeled though an allometrically scaled clearance constant,

$$\begin{aligned} \frac{\text{d}A_{KE}^{j}}{\text{d}t} &= k_R^j \cdot C_A^j \\ k_R^j &= k_{R0}^j \cdot \text{BW} \end{aligned} \tag{8}$$

Here, k_R^j is the rate of renal clearance of the chemical; j represents APAP, APAP-G, or APAP-S; k_{R0}^j are baseline values that are scaled allometrically by body weight. Biliary clearance was neglected because APAP and APAP-S are not excreted into the bile, and APAP-G is only excreted in trace amounts (Jayasinghe et al. 1986).

2.2.5 PBPK model equations

Combining the above species mass balance equations and mechanistic relationships results in the governing equations comprising the mathematical expression of the PBPK model. This system of differential and algebraic equations is summarized in Table 4.

2.3 Parameter estimation and model simulations

Unknown model parameters in the governing equations were estimated within the context of a Bayesian hierarchical framework (Lyons et al. 2008; Chiu et al. 2009). The hierarchy consisted of two levels: a population level, comprising an aggregation of all of the training set data

Table 4 System of governing equations for the PBPK model

	APAP	APAP-G	APAP-S
Fat	$\frac{dC_{fat}^{APAP}}{dt} = \frac{Q_{fat}\left(C_A^{APAP} - C_{V-fat}^{APAP}\right)}{V_{fat}}$	$\frac{dC_{fat}^{APAP-G}}{dt} = \frac{Q_{fat}\left(C_A^{APAP-G} - C_{V-fat}^{APAP-G}\right)}{V_{fat}}$	$\frac{dC_{fat}^{APAP-S}}{dt} = \frac{Q_{fat}\left(C_A^{APAP-S} - C_{V-fat}^{APAP-S}\right)}{V_{fat}}$
Muscle	$\frac{dC_{muscle}^{APAP}}{dt} = \frac{Q_{muscle}\left(C_A^{APAP} - C_{V-muscle}^{APAP}\right)}{V_{muscle}}$	$\frac{dC_{muscle}^{APAP-G}}{dt} = \frac{Q_{muscle}\left(C_A^{APAP-G} - C_{V-muscle}^{APAP-G}\right)}{V_{muscle}}$	$\frac{dC_{muscle}^{APAP-S}}{dt} = \frac{Q_{muscle}\left(C_A^{APAP-S} - C_{V-muscle}^{APAP-S}\right)}{V_{muscle}}$
Liver	$\frac{dC_{liver}^{APAP}}{dt} = \frac{Q_{liver}\left(C_A^{APAP} - C_{V-liver}^{APAP}\right) - v_{cyp} - v_{APAP-G} - v_{APAP-S}}{V_{liver}}$	$\frac{dC_{liver}^{APAP-G}}{dt} = \frac{Q_{liver}\left(C_A^{APAP-G} - C_{V-liver}^{APAP-G}\right) + v_{mem-APAP-G}}{V_{liver}}$	$\frac{dC_{liver}^{APAP-S}}{dt} = \frac{Q_{liver}\left(C_A^{APAP-S} - C_{V-liver}^{APAP-S}\right) + v_{mem-APAP-S}}{V_{liver}}$
Hepatocyte	–	$\frac{dA_{hep}^{APAP-G}}{dt} = v_{APAP-G} - v_{mem}^{APAP-G}$	$\frac{dA_{hep}^{APAP-S}}{dt} = v_{APAP-S} - v_{mem}^{APAP-S}$
Kidney	$\frac{dC_{kidney}^{APAP}}{dt} = \frac{\frac{dA_{glx}}{dt} + Q_{kidney}\left(C_A^{APAP} - C_{V-kidney}^{APAP}\right) - k_R^{APAP} \cdot C_A^{APAP}}{V_{kidney}}$	$\frac{dC_{kidney}^{APAP-G}}{dt} = \frac{Q_{kidney}\left(C_A^{APAP-G} - C_{V-kidney}^{APAP-G}\right) - k_R^{APAP-G} \cdot C_A^{APAP-G}}{V_{kidney}}$	$\frac{dC_{kidney}^{APAP-S}}{dt} = \frac{Q_{kidney}\left(C_A^{APAP-S} - C_{V-kidney}^{APAP-S}\right) - k_R^{APAP-S} \cdot C_A^{APAP-S}}{V_{kidney}}$
GI	$\frac{dA_{GI}^{APAP}}{dt} = I(t) - \frac{M\left[\exp\left(\frac{-t}{T_G}\right) - \exp\left(\frac{-t}{T_P}\right)\right]}{T_G - T_P}$	–	–
Slowly perfused	$\frac{dC_{sp}^{APAP}}{dt} = \frac{Q_{sp}\left(C_A^{APAP} - C_{V-sp}^{APAP}\right)}{V_{sp}}$	$\frac{dC_{sp}^{APAP-G}}{dt} = \frac{Q_{sp}\left(C_A^{APAP-G} - C_{V-sp}^{APAP-G}\right)}{V_{sp}}$	$\frac{dC_{sp}^{APAP-S}}{dt} = \frac{Q_{sp}\left(C_A^{APAP-S} - C_{V-sp}^{APAP-S}\right)}{V_{sp}}$
Rapidly perfused	$\frac{dC_{rp}^{APAP}}{dt} = \frac{Q_{rp}\left(C_A^{APAP} - C_{V-rp}^{APAP}\right)}{V_{rp}}$	$\frac{dC_{rp}^{APAP-G}}{dt} = \frac{Q_{rp}\left(C_A^{APAP-G} - C_{V-rp}^{APAP-G}\right)}{V_{rp}}$	$\frac{dC_{rp}^{APAP-S}}{dt} = \frac{Q_{rp}\left(C_A^{APAP-S} - C_{V-rp}^{APAP-S}\right)}{V_{rp}}$
Urine	$\frac{dA_e^{APAP}}{dt} = k_R^{APAP} \cdot C_A^{APAP}$	$\frac{dA_e^{APAP-G}}{dt} = k_R^{APAP-G} \cdot C_A^{APAP-G}$	$\frac{dA_e^{APAP-S}}{dt} = k_R^{APAP-S} \cdot C_A^{APAP-S}$
Arterial blood concentration	$\frac{dC_{BLA}^{APAP}}{dt} = \frac{Q_C\left(C_V^{APAP} - C_A^{APAP}\right)}{V_{BLA}}$ $C_A^{APAP} = \frac{A_A^{APAP}}{V_{BLA}}$	$\frac{dC_{BLA}^{APAP-G}}{dt} = \frac{Q_C\left(C_V^{APAP-G} - C_A^{APAP-G}\right)}{V_{BLA}}$ $C_A^{APAP-G} = \frac{A_A^{APAP-G}}{V_{BLA}}$	$\frac{dC_{BLA}^{APAP-S}}{dt} = \frac{Q_C\left(C_V^{APAP-S} - C_A^{APAP-S}\right)}{V_{BLA}}$ $C_A^{APAP-S} = \frac{A_A^{APAP-S}}{V_{BLA}}$
Venous blood concentration (pooled)	$\frac{dC_{BLV}^{APAP}}{dt} = \frac{\sum_T Q_T C_{V-T}^{APAP} - Q_C C_V^{APAP} + D_{IV}(t)}{V_{BLV}}$, $C_V^{APAP} = \frac{A_V^{APAP}}{V_{BLV}}$ where $D_{IV}(t)$ is the rate of intravenous APAP dosing	$\frac{dC_{BLV}^{APAP-G}}{dt} = \frac{\sum_T Q_T C_{V-T}^{APAP-G} - Q_C C_V^{APAP-G}}{V_{BLV}}$ $C_V^{APAP-G} = \frac{A_V^{APAP-G}}{V_{BLV}}$	$\frac{dC_{BLV}^{APAP-S}}{dt} = \frac{\sum_T Q_T C_{V-T}^{APAP-S} - Q_C C_V^{APAP-S}}{V_{BLV}}$ $C_V^{APAP-S} = \frac{A_V^{APAP-S}}{V_{BLV}}$

Table 5 Parameter descriptions and prior distributions

Description	Parameter (units)	Distribution	References
Acetaminophen absorption			
Gastric emptying time constant	T_G (h)	N (0.23, 0.5)	Levitt (2013)
GI perfusion time constant	T_P (h)	N (0.033, 0.5)	Levitt (2013)
Phase I metabolism			
Cytochrome P450 K_M	K_{M-cyp}^{APAP} (μM)	N (130, 1)	Laine et al. (2009)
Cytochrome P450 V_{max}	V_{MC-cyp} (μmol/h-BW$^{0.75}$)	U (0.14, 2900)	–
Phase II metabolism: sulfation			
Sulfation pathway acetaminophen K_M	K_{M-sult}^{APAP} (μM)	N (300, 1)	Riches and Bloomer (2009)
Sulfation pathway substrate inhibition K_i	K_{I-sult}^{APAP} (μM)	N (526, 1)	Nagar et al. (2006)
Sulfation pathway PAPS K_M	K_{M-sult}^{PAPS} (unitless)	N (0.5, 0.5)	–
Sulfation pathway acetaminophen V_{max}	$V_{MC-sult}$ (μmol/h-BW$^{0.75}$)	U (1, 3.26E6)	–
Phase I metabolism: glucuronidation			
Glucuronidation pathway acetaminophen K_M	K_{M-ugt}^{APAP} (μM)	N (6.0E4, 1)	Riches and Bloomer (2009)
Glucuronidation pathway substrate inhibition K_i	K_{I-ugt}^{APAP} (μM)	N (5.8E4, 0.25)	Mutlib et al. (2006)
Glucuronidation pathway GA K_M	K_{M-sult}^{UDPGA} (unitless)	N (0.5, 0.5)	–
Glucuronidation pathway acetaminophen V_{max}	V_{MC-ugt} (μmol/h-BW$^{0.75}$)	U (1, 3.26E6)	–
Active hepatic transporters			
APAP-G hepatic transporter K_M	K_{M-mem}^{APAP-G} (μM)	N (1.99E4, 0.3)	Iida (1989)
APAP-G hepatic transporter V_M	V_{M-mem}^{APAP-G} (μmol/h)	U (1.09E3, 3.26E6)	–
APAP-S hepatic transporter K_M	K_{M-mem}^{APAP-S} (μM)	N (2.29E4, 0.22)	Iida (1989)
APAP-S hepatic transporter V_M	V_{M-mem}^{APAP-S} (μmol/h)	U (1.09E3, 3.26E6)	–
Cofactor synthesis			
UDPGA synthesis	$k_{syn-UDPGA}$ (1/h)	U (1, 4.43E5)	–
PAPS synthesis	$k_{syn-PAPS}$ (1/h)	U (1, 4.43E5)	–
Clearance			
Acetaminophen clearance	k_{R0}^{APAP} (L/h-BW$^{0.75}$)	U (2.48E − 3, 2.718)	–
Acetaminophen-glucuronide clearance	k_{R0}^{APAP-G} (L/h-BW$^{0.75}$)	U (2.48E−3, 2.718)	–
Acetaminophen-sulfate clearance	k_{R0}^{APAP-S} (L/h-BW$^{0.75}$)	U (2.48E−3, 2.718)	–

N (a, b) denotes a normal distribution with mean, a, and coefficient of variation, b; U (a, b) denotes a uniform distribution with minimum and maximum values a and b, respectively

across all of the studies, and a study level, consisting of all of the separate training set studies. Using this methodology, inter-study variability could be accounted for, and pharmacokinetic predictions and parameter distributions could be found and compared at both levels within the hierarchy.

Within the framework, the parameter space was sampled using a Markov chain Monte Carlo (MCMC) method (Gelman 2011) using three independent Markov chains per simulation. Distributions for parameter priors were based on values from the literature when available and were assumed to be uniform distributions over biologically plausible ranges otherwise. Markov chains were run for 100,000 iterations per chain, and convergence was assessed using a Gelman-Rubin reduction factor (Gelman 2011) with a maximum threshold of $R = 1.05$. Posterior parameter distributions were computed from the final 30,000 iterations of each chain. For each of these final iterations, the complete set of parameter values was recorded as an individual "setpoint" (Bois 2009).

Following parameterization, the governing equation system was solved at dosing scenarios of interest using all of the 30,000 setpoints, leading to a family of simulation results that was used subsequently to illustrate predictions for a variety of pharmacokinetics measures of interest and quantify the uncertainty associated with these values.

2.4 Software and computing platform

Data available from the literature in graphical form were digitized using DigitizeIt v.1.5.8 (Bormann et al. 2015). Simulations of the governing equation system, including

the MCMC and setpoint analyses, were conducted using MCSim v5.4 (Bois 2009). Processing, analysis, and visualization of data and simulation results were carried out using scripts written in Python v.2.7.2 (Python Software Foundation 2015), utilizing the numpy (Van der Walt et al. 2011), scipy (Jones et al. 2001), and matplotlib (Hunter 2007) packages. All calculations were performed on a computer cluster running the 64-bit CentOS Linux operating system on six-gigabit linked Dell 2950 servers, each containing two quad-core 2.5-GHz Xeon processors and 64 GB of RAM.

3 Results and discussion

3.1 Model parameter values

Using time-course plasma and urinary data from the designated training set of studies (Table 1), and the priors listed in Table 5, distributions for the unknown parameters in the governing equations were computed through the Bayesian framework described earlier. The resulting posterior distributions for each parameter are summarized in Table 6. As described, setpoint analyses were then conducted to accumulate a large family of simulation results indicative of the data uncertainty and inter-study variability realized in these parameter distributions. These results were subsequently used in the various comparisons and predictions shown below.

3.2 Model validation and testing

To validate the PBPK model, several comparisons and assessments were made. For convenience in evaluating these comparisons, both the appropriate training set data (used in the model calibration) and test set data (reserved for validation) from Table 1 are shown in subsequent plots. The former points are presented so that the accuracy of the parameter estimation can be assessed, while the latter can be used to evaluate the predictive nature of the model.

First, model predictions for time-course plasma concentrations of APAP, APAP-G, and APAP-S were compared to experimental values obtained from the literature. As shown in Fig. 3, there is generally good agreement between predicted and measured values of the time-course concentrations for both the parent chemical and its metabolites over a wide range of data obtained from numerous studies. These simulations also illustrate the degree of uncertainty in the model predictions based on parameterization to data from a diverse set of studies.

The ability of the model to accurately simulate renal clearance was then evaluated. There are relatively few studies in humans detailing the amount of APAP and its metabolites in the urine over time. Here, available time-course data (Critchley et al. 1986; Lau and Critchley 1994; Prescott 1980; Tan et al. 2012) were used as the training set for model calibration, while data at the terminal time point of 24 h (Critchley et al. 2005; Esteban et al. 1996; Kamali 1993) were applied as the test set. As shown in Fig. 4, model and experimental results at 24 h are in satisfactory to good agreement for the accumulated amounts of all three chemical species. Future studies quantifying the time course amounts of APAP and its metabolites in the urine would further reduce the uncertainty in these predictions.

Next, model predictions of APAP absorption into the bloodstream were assessed. Figure 5 shows simulated values of the cumulative fraction absorbed (CFA), along with corresponding in vivo data from Souliman et al. (2006), for a 500-mg oral dose of APAP administered to humans in a fasted state. The good agreement between model predictions

Table 6 Posterior distributions for parameters

Parameter (units)	Value
Acetaminophen absorption	
T_G (h)	0.332 (0.36)
T_P (h)	0.0476 (0.30)
Phase I metabolism	
K_{M-cyp}^{APAP} (μM)	123 (0.29)
V_{MC-cyp} (μmol/h-BW$^{0.75}$)	2.57 (0.87)
Phase II metabolism: sulfation	
K_{M-sult}^{APAP} (μM)	1.2E3 (0.39)
K_{I-sult}^{APAP} (μM)	478 (0.25)
K_{M-sult}^{PAPS} (unitless)	0.345 (0.40)
$V_{MC-sult}$ (μmol/h-BW$^{0.75}$)	467 (0.38)
Phase II metabolism: glucuronidation	
K_{M-ugt}^{APAP} (μM)	6.14E3 (0.33)
K_{I-ugt}^{APAP} (μM)	4.99E4 (0.26)
K_{M-sult}^{UDPGA} (unitless)	0.343 (0.38)
V_{MC-ugt} (μmol/h-BW$^{0.75}$)	5.21E3 (0.31)
Active hepatic transporters	
K_{M-mem}^{APAP-G} (μM)	1.75E4 (0.27)
V_{M-mem}^{APAP-G} (μmol/h)	3.54E4 (0.45)
K_{M-mem}^{APAP-S} (μM)	2.23E4 (0.20)
V_{M-mem}^{APAP-S} (μmol/h)	1.4E7 (1.65)
Cofactor synthesis	
$k_{syn-UDPGA}$ (1/h)	3.6E4 (0.87)
$k_{syn-PAPS}$ (1/h)	3.66E3 (0.69)
Clearance	
k_{R0}^{APAP} (L/h-BW$^{0.75}$)	0.0123 (0.35)
k_{R0}^{APAP-G} (L/h-BW$^{0.75}$)	0.155 (0.22)
k_{R0}^{APAP-S} (L/h-BW$^{0.75}$)	0.138 (0.28)

Values are reported as the mean (coefficient of variation) of the distribution

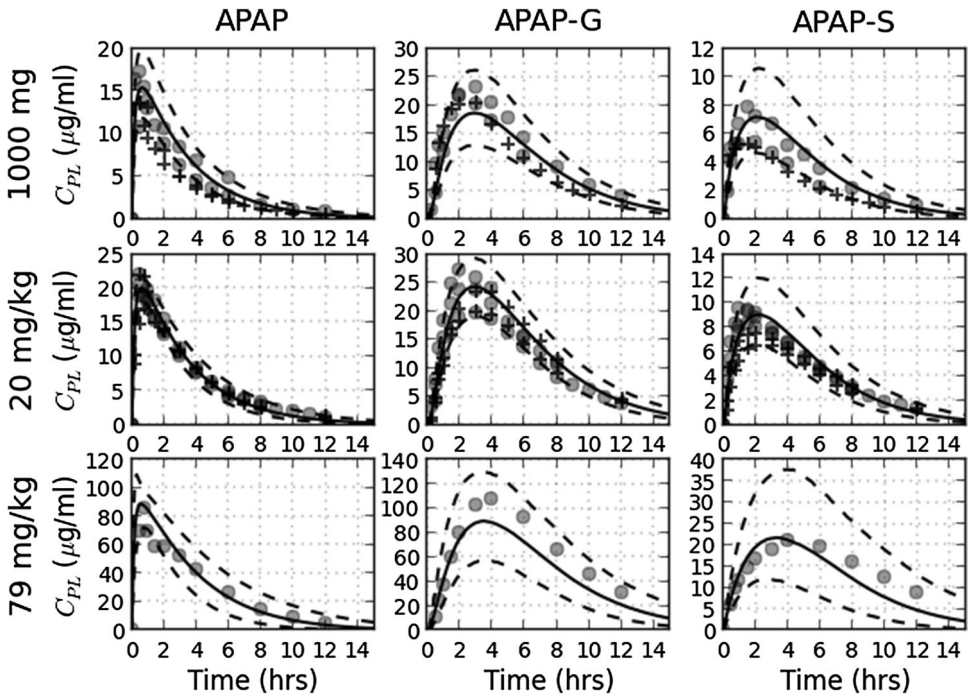

Fig. 3 Comparison of model simulations results to human plasma concentration data following oral dosing of APAP. Simulation results are shown with a *solid line* for mean values and *dashed lines* representing 95 % confidence intervals. Data from the training set are represented by *circles*, while those from the test are represented by the *plus sign*

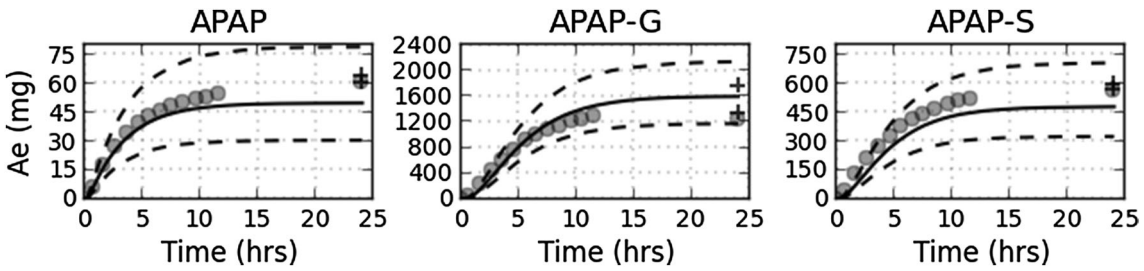

Fig. 4 Comparison of model simulation results to experimental data for the accumulated amount of APAP in the urine following a 20 mg/kg oral dose

and experimental data lends support to the quantitative description of absorption used in the PBPK model. However, although not explicitly tested in this study, if simulations for dosages outside of the clinical range (e.g., overdose) are to be conducted, it is anticipated that the time constants in the model for gastric emptying and gut perfusion may need to be adjusted or made dose dependent.

Finally, comparisons were made with respect to several common pharmacokinetic parameters: AUC, C_{max}, mean residence time (MRT), and fraction excreted. Table 7 lists mean values and uncertainties of these measures for a single oral dose of 20 mg/kg of APAP. Because the data values (Critchley et al. 2005) were part of the test set enumerated in Table 1 and were not used in model calibration, the good agreement between simulation-based and experimentally derived values for all measures and chemical species provides evidence of the accuracy of the PBPK model in predicting these summary parameters within the uncertainties of the system.

3.3 Model predictions

To demonstrate its utility for elucidating and quantifying the ADME of APAP, several predicted outputs and endpoints of interest are illustrated in the following sections: cofactor depletion, dose dependence of pharmacokinetic parameters, and the relationship between APAP levels in the plasma to those in the liver.

3.3.1 Cofactor depletion

Because acetaminophen is rapidly metabolized to APAP-G and APAP-S, associated cofactors may be quickly depleted, thus reducing the rate of acetaminophen conjugation. For example, the PAPS cofactor has been reported to deplete under therapeutic dosing conditions, reducing the rate of acetaminophen clearance (Critchley et al. 1986). In addition, since sulfation and glucuronidation are common during phase II metabolism of many xenobiotics (Volak

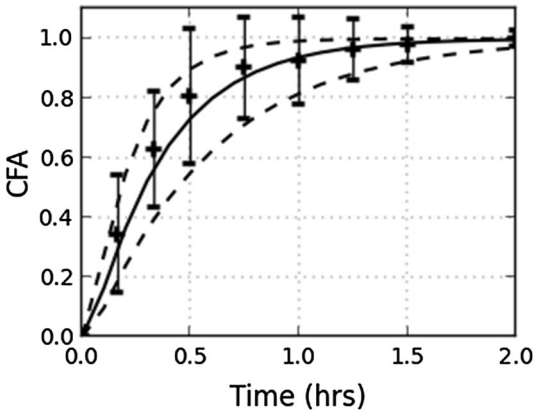

Fig. 5 Cumulative fraction absorbed (CFA) of APAP into the bloodstream. Simulation results are shown with a *solid line* for mean values and *dashed lines* representing 95 % confidence intervals. *Plus signs* represent data from the literature and were not part of the training set

et al. 2013), cofactor depletion may be an important consideration for the co-administration of other drugs with APAP. Figure 6 depicts model simulations for cofactor depletion following APAP administration. The predicted time frame for PAPS and UDPGA depletion in the liver agrees with that from Hjelle et al. (1985), where the majority of cofactor is depleted 30–60 min post-acetaminophen dosing. The insets in Fig. 6 show the predicted values of the minimum fraction of cofactor available, ϕ^{PAPS} and ϕ^{UDPGA}, at various clinically relevant doses. Data quantifying the dose dependency of cofactor depletion in humans could not be found in the literature; however, the trends seen in these insets are similar to those for reduction in PAPS and UDPGA observed in an experimental study in rats (Hjelle et al. 1985).

3.3.2 *Dose-dependent pharmacokinetic parameters*

Understanding the variation in a drug's pharmacokinetic parameters with respect to dose can help to inform its safe and effective administration. Figure 7 shows model predictions of the dose dependence of two important pharmacokinetic metrics for APAP: AUC and mean residence time (MRT) in both the plasma and liver. Consistent with results from the literature (Sahajwalla and Ayres 1991), predictions from the PBPK model indicate a linear dose dependence for these metrics over a range of common therapeutic oral doses, but show deviations from this linear trend at doses above about 60 mg/kg. These latter simulation results are indicative of saturation of the sulfation and glucoronidation pathways through depletion of the metabolic cofactors (see Sect. 3.3.1) and are in accord with results from previous experimental studies (Lin 1994; Hjelle and Klaassen 1984; Tone et al. 1990).

Table 7 Comparison of pharmacokinetic parameters from experiments and model simulations

	Experiments	Model simulations
APAP		
C_{max} (μg/ml)	21.51 (14.4–32.3)	20.50 (16.45–28.93)
AUC (μg/ml/h)	83.16 (50.8–117.1)	83.09 (49.56–128.62)
MRT (h)	3.21 (3.01–3.51)	3.45 (2.41–4.69)
CL_R (ml/min)	11.52 (4.5–18.1)	13.27 (6.75–26.09)
% Recovery	5.03 (2.4–9.0)	5.06 (1.51–10.27)
APAP-G		
C_{max} (μg/ml)	10.27 (5.8–15.1)	11.43 (6.82–17.04)
AUC (μg/ml/h)	82.68 (50.9–119.5)	87.65 (55.33–135.66)
MRT (h)	6.18 (5.18–6.77)	5.76 (4.40–7.58)
CL_R (ml/min)	133.95 (82–187)	169.51 (107.46–267.41)
% Recovery	57.21 (40.7–68.6)	68.77 (51.66–85.94)
APAP-S		
C_{max} (μg/ml)	5.18 (3.15–7.41)	5.64 (2.79–10.32)
AUC (μg/ml/h)	38.74 (24.2–62)	38.28 (16.61–79.78)
MRT (h)	5.91 (5.35–6.49)	4.91 (3.55–6.42)
CL_R (ml/min)	153.4 (85–217)	158.35 (94.18–266.24)
% Recovery	31.28 (19.8–46.4)	27.73 (11.51–45.61)

Tabulated values presented in the "Experiments" columns were taken directly from Critchley et al. (2005), except for MRT, which was computed from digitized data extracted from the same reference

3.3.3 *Relating APAP levels in the plasma to those in the liver*

Although the putative species responsible for hepatotoxicity is NAPQI and not APAP, assessment of potential acetaminophen toxicity is currently based on knowledge of the administered dose or the APAP level measured in the plasma (Rumack 2002). Even when using the level of APAP as a measure of potential hepatotoxicity, the concentration in the liver is expected to be a more representative dose metric than that present elsewhere in the body. To estimate this concentration, however, requires a method to associate it with a more readily measurable quantity, such as the amount of APAP or its metabolite in the plasma. This predictive relationship could be deduced by comparing and connecting concentration-time profiles for these species. Figure 8 depicts an alternative approach, in which each trace or trajectory provides a direct means of estimating $C_{\mathrm{liver}}^{\mathrm{APAP}}$ given a value of C_{plasma} for one (or more) of APAP, APAP-G, or APAP-S and some knowledge of the time after dosing. Additionally, from a qualitative perspective, these plots characterize the relationship between the pharmacokinetics of the two chemicals. For instance, each trajectory in this figure is visually segmented to give a rough indication of regions of shared pharmacokinetic processes:

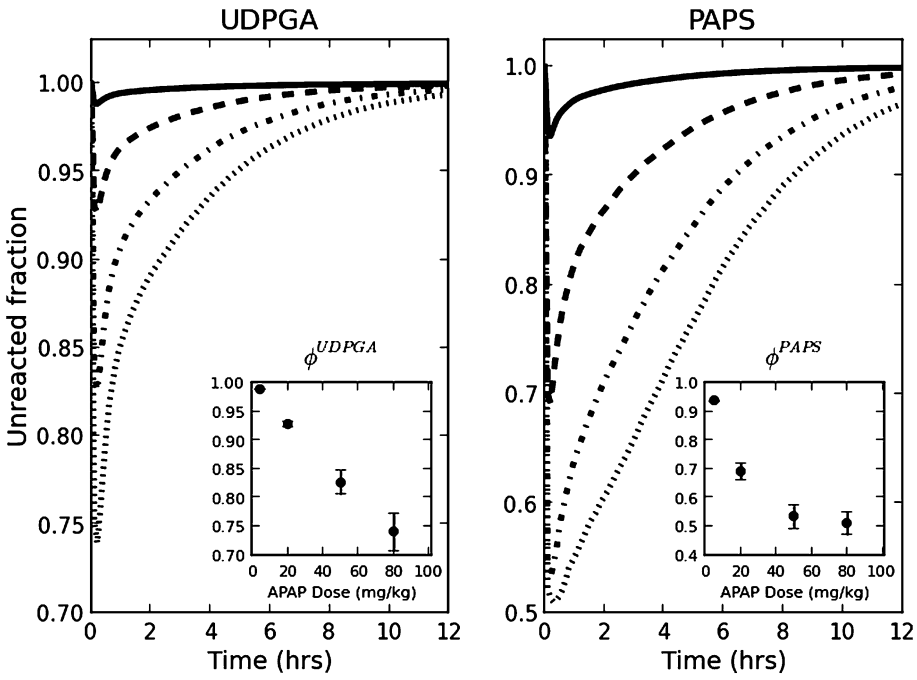

Fig. 6 Model prediction of depletion of the cofactors UDPGA and PAPS. *Insets* depict the predicted the dose response for the minimum available cofactor following APAP administration

	Plasma		Liver
	APAP	APAP-G, APAP-S	APAP
Solid line	Absorption	Formation	Absorption
Dotted line	Absorption	Formation	Elimination
Dashed line	Elimination	Elimination	Elimination

Furthermore, the trajectory's deviation from the diagonal and degree of diagonal indicate the gross differences in the magnitude and time scale for the ADME of the plasma and liver species, and the length of the dotted portion of a curve expresses the difference in the time at which C_{max} occurs (t_{max}).

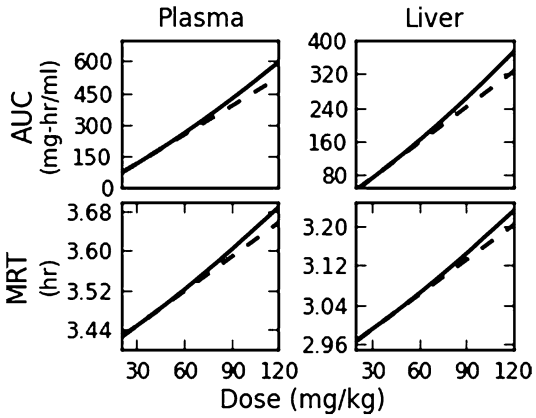

Fig. 7 Model prediction of the dose dependence of pharmacokinetic measures for APAP in the plasma and the liver compartment: AUC and mean residence time (MRT). *Dashed lines* represent a linear response with respect to dose

4 Conclusions

The primary objective of this study was to create a physiologically based pharmacokinetic model for acetaminophen ADME in humans, supported by a broad set of experimental data from the literature. Once developed and validated, this model enabled the simulation of the disposition of APAP and two of its key metabolites, APAP-G and APAP-S, in plasma, urine, and several pharmacologically and toxicologically relevant tissues, and it included information to compute the uncertainty in these predictions. Although not commonly measured clinically, the metabolites examined here have markedly different pharmacokinetic profiles than that of the parent drug, and their levels provide additional and complementary information useful in estimating the APAP dose and internal tissue concentrations. Because the model is based on physiological and biochemical relationships, we anticipate that it will be useful in a number of applications, such as dose extrapolation studies, determining the tissue-specific pharmacokinetics of APAP in susceptible, vulnerable, or health-compromised populations, assessing the pharmacokinetic impact of co-administration of another drug, relating measured biomarker levels to internal concentrations, and estimating the administered dose using concentrations measured in plasma and urine. Finally, if integrated with

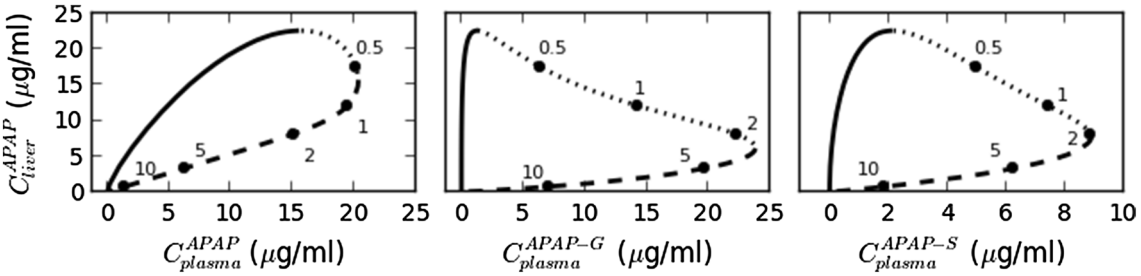

Fig. 8 Model prediction of the relationship between plasma levels of the parent compound and conjugates and parent APAP in the liver for a 20 mg/kg dose. Time increases in the clockwise direction around the trajectory loops, and numbers shown correspond to the number of hours post dosing. *Line styles* are described in the text

appropriate pharmacodynamic equations and relationships, the present model could be used to help predict and characterize APAP toxicity.

Acknowledgments The authors wish to thank the staff at the Franklin A. Graybill Statistical Laboratory at Colorado State University for their advice and consultation on several issues related to statistical analysis.

References

Ameer B, Greenblatt DJ, Divoll M, Abernethy DR, Shargel L (1981) High-performance liquid chromatographic determination of acetaminophen in plasma: single-dose pharmacokinetic studies. J Chromatogr 226:224–230

Ben-Shachar R, Chen Y, Luo S, Hartman C, Reed M, Nijhout HF (2012) The biochemistry of acetaminophen hepatotoxicity and rescue: a mathematical model. Theor Biol Med Model 9:55

Bois FY (2009) GNU MCSim: Bayesian statistical inference for SBML-coded systems biology models. Bioinformatics 25:1453–1454

Brown RP, Delp MD, Lindstedt SL, Rhomberg LR, Beliles RP (1997) Physiological parameter values for physiologically based pharmacokinetic models. Toxicol Ind Health 13:407–484

Campbell JL, Clewell RA, Gentry PR, Andersen ME, Clewell HJ (2012) Physiologically based pharmacokinetic/toxicokinetic modeling. Methods Mol Biol 929:439–499

Chan MT, Anderson PJ, Chan JC, Lau GS, Critchley JA (1997) Single-dose pharmacokinetics of paracetamol and its conjugates in Chinese non-insulin-dependent diabetic patients with renal impairment. Eur J Clin Pharmacol 52:285–288

Chen L, Mohr SN, Yang CS (1996) Decrease of plasma and urinary oxidative metabolites of acetaminophen after consumption of watercress by human volunteers. Clin Pharmacol Ther 60:651–660

Chiew A, Day P, Salonikas C, Naidoo D, Graudins A, Thomas R (2010) The comparative pharmacokinetics of modified-release and immediate-release paracetamol in a simulated overdose model. Emerg Med Aust 22:548–555

Chiu WA, Okino MS, Evans MV (2009) Characterizing uncertainty and population variability in the toxicokinetics of trichloroethylene and metabolites in mice, rats, and humans using an updated database, physiologically based pharmacokinetic (PBPK) model, and Bayesian approach. Toxicol Appl Pharmacol Elsevier BV 241:36–60

Clements JA, Heading RC, Nimmo WS, Prescott LF (1978) Kinetics of acetaminophen absorption and gastric emptying in man. Clin Pharmacol Ther 24:420–431

Clements JA, Critchley JA, Prescott LF (1984) The role of sulphate conjugation in the metabolism and disposition of oral and intravenous paracetamol in man. Br J Clin Pharmacol 18:481–485

Critchley JA, Nimmo GR, Gregson CA, Woolhouse NM, Prescott LF (1986) Inter-subject and ethnic differences in paracetamol metabolism. Br J Clin Pharmacol 22:649–657

Critchley JA, Critchley LA, Anderson PJ, Tomlinson B (2005) Differences in the single-oral-dose pharmacokinetics and urinary excretion of paracetamol and its conjugates between Hong Kong Chinese and Caucasian subjects. J Clin Pharm Ther 30:179–184

Edginton AN, Schmitt W, Willmann S (2006) Development and evaluation of a generic physiologically based pharmacokinetic model for children. Clin Pharmacokinet 45:1013–1034

Esteban A, Calvo R, Pérez-Mateo M (1996) Paracetamol metabolism in two ethnically different Spanish populations. Eur J Drug Metab Pharmacokinet 21:233–239

Fong BM, Siu TS, Tam S (2011) Persistently increased acetaminophen concentrations in a patient with acute liver failure. Clin Chem 57:9–11

Forrest JA, Clements JA, Prescott LF (1982) Clinical pharmacokinetics of paracetamol. Clin Pharmacokinet 7:93–107

Geenen S, Yates JWT, Kenna JG, Bois FY, Wilson ID, Westerhoff HV (2013) Multiscale modelling approach combining a kinetic model of glutathione metabolism with PBPK models of paracetamol and the potential glutathione-depletion biomarkers ophthalmic acid and 5-oxoproline in humans and rats. Integr Biol (Camb) 5:877–888

Gelman A, Shirley K (2011) Inference from simulations and monitoring convergence. In: Brooks S, Gelman A, Jones GL, Meng X-L (eds) Handb. Markov Chain Monte Carlo. Chapman and Hall, UK, pp 163–174

Gwilt J, Robertson A, McChesney E (1963) Determination of blood and other tissue concentrations of paracetamol in dog and man. J Pharm Pharmacol 15:440–444

Hjelle JJ, Klaassen CD (1984) Glucuronidation and biliary excretion of acetaminophen in rats. J Pharmacol Exp Ther 228:407–413

Hjelle JJ, Hazelton GA, Klaassen CD (1985) Acetaminophen decreases adenosine 3′-phosphate 5′-phosphosulfate and uridine diphosphoglucuronic acid in rat liver. Drug Metab Dispos 13:35–41

Hunter JD (2007) Matplotlib: a 2D graphics environment. Comput Sci Eng 9:90–95

Iida S, Mizuma T, Sakuma N, Hayashi M, Awazu S (1989) Transport of acetaminophen conjugates in isolated rat hepatocytes. Drug Metab Dispos 17:341–344

Itoh H, Nagano T, Takeyama M (2002) Effect of nizatidine on paracetamol and its metabolites in human plasma. J Pharm Pharmacol 54:869–873

Jayasinghe KS, Roberts CJ, Read AE (1986) Is biliary excretion of paracetamol significant in man? Br J Clin Pharmacol 22:363–366

Jensen LS, Valentine J, Milne RW, Evans AM (2004) The quantification of paracetamol, paracetamol glucuronide and paracetamol sulphate in plasma and urine using a single high-performance liquid chromatography assay. J Pharm Biomed Anal 34:585–593

Jones E, Oliphant TE, Peterson P (2001) SciPy: open source scientific tools for Python. http://www.scipy.org/

Kamali F (1993) The effect of probenecid on paracetamol metabolism and pharmacokinetics. Eur J Clin Pharmacol 45:551–553

Kim D-W, Tan EY, Jin Y, Park S, Hayes M, Demirhan E et al (2011) Effects of imatinib mesylate on the pharmacokinetics of paracetamol (acetaminophen) in Korean patients with chronic myelogenous leukaemia. Br J Clin Pharmacol 71:199–206

Laine JE, Auriola S, Pasanen M, Juvonen RO (2009) Acetaminophen bioactivation by human cytochrome P450 enzymes and animal microsomes. Xenobiotica 39:11–21

Lau GS, Critchley JA (1994) The estimation of paracetamol and its major metabolites in both plasma and urine by a single high-performance liquid chromatography assay. J Pharm Biomed Anal 12:1563–1572

Levitt DG (2013) Quantitation of small intestinal permeability during normal human drug absorption. BMC Pharmacol Toxicol 14:34

Lin JH (1994) Dose-dependent pharmacokinetics: experimental observations and theoretical considerations. Biopharm Drug Dispos 15:1–31

Lin J, Lu A (1997) Role of pharmacokinetics and metabolism in drug discovery and development. Pharmacol Rev 49:403–449

Lyons MA, Yang RSH, Mayeno AN, Reisfeld B (2008) Computational toxicology of chloroform: reverse dosimetry using Bayesian inference, Markov chain Monte Carlo simulation, and human biomonitoring data. Environ Health Perspect 116:1040–1046

Marangoni AG (2002) Enzyme kinetics. Wiley, USA

Martin U, Temple RM, Winney RJ, Prescott LF (1993) The disposition of paracetamol and its conjugates during multiple dosing in patients with end-stage renal failure maintained on haemodialysis. Eur J Clin Pharmacol 45:141–145

Morris ME, Levy G (1984) Renal clearance and serum protein binding of acetaminophen and its major conjugates in humans. J Pharm Sci 73:1038–1041

Mutlib AE, Goosen TC, Bauman JN, Williams JA, Kulkarni S, Kostrubsky S (2006) Kinetics of acetaminophen glucuronidation by UDP-glucuronosyltransferases 1A1, 1A6, 1A9 and 2B15. Potential implications in acetaminophen-induced hepatotoxicity. Chem Res Toxicol 19:701–709

Nagar S, Walther S, Blanchard RL (2006) Sulfotransferase (SULT) 1A1 polymorphic variants *1, *2, and *3 are associated with altered enzymatic activity, cellular phenotype, and protein degradation. Mol Pharmacol 69:2084–2092

Naritomi Y, Terashita S, Kagayama A, Sugiyama Y (2003) Utility of hepatocytes in predicting drug metabolism: comparison of hepatic intrinsic clearance in rats and humans in vivo and in vitro. Drug Metab Dispos 31:580–588

Navid A, Ng DM, Stewart BJ, Wong SE, Lightstone FC (2013) Quantitative In Silico analysis of transient metabolism of acetaminophen and associated causes of hepatotoxicity in humans. In Silico Pharmacol 1:14

Péry ARR, Brochot C, Zeman FA, Mombelli E, Desmots S, Pavan M et al (2013) Prediction of dose-hepatotoxic response in humans based on toxicokinetic/toxicodynamic modeling with or without in vivo data: a case study with acetaminophen. Toxicol Lett Elsevier Ireland Ltd. 220:26–34

Peters SA (2012) Physiologically-based pharmacokinetic (PBPK) modeling and simulations. Wiley, USA

Prescott LF (1980) Kinetics and metabolism of paracetamol and phenacetin. Br J Clin Pharmacol 10(Suppl 2):291S–298S

Prescott LF, Speirs GC, Critchley JA, Temple RM, Winney RJ (1989) Paracetamol disposition and metabolite kinetics in patients with chronic renal failure. Eur J Clin Pharmacol 36:291–297

Rawlins MD, Henderson DB, Hijab AR (1977) Pharmacokinetics of paracetamol (acetaminophen) after intravenous and oral administration. Eur J Clin Pharmacol 11:283–286

Reisfeld B, Mayeno AN, Lyons MA, Yang RSH (2007) Computational toxicology. In: Ekins S (ed) Wiley, USA, pp. 33–69

Riches Z, Bloomer J, Patel a, Nolan a, Coughtrie M (2009) Assessment of cryopreserved human hepatocytes as a model system to investigate sulfation and glucuronidation and to evaluate inhibitors of drug conjugation. Xenobiotica 39:374–381

Rodgers T, Rowland M (2006) Physiologically based pharmacokinetic modelling 2: predicting the tissue distribution of acids, very weak bases, neutrals and zwitterions. J Pharm Sci 95:1238–1257

Rumack BH (2002) Acetaminophen hepatotoxicity: the first 35 years. J Toxicol Clin Toxicol 40:3–20

Sahajwalla CG, Ayres JW (1991) Multiple-dose acetaminophen pharmacokinetics. J Pharm Sci 80:855–860

Shinoda S, Aoyama T, Aoyama Y, Tomioka S, Matsumoto Y, Ohe Y (2007) Pharmacokinetics/pharmacodynamics of acetaminophen analgesia in Japanese patients with chronic pain. Biol Pharm Bull 30:157–161

Souliman S, Blanquet S, Beyssac E, Cardot J-M (2006) A level A in vitro/in vivo correlation in fasted and fed states using different methods: applied to solid immediate release oral dosage form. Eur J Pharm Sci 27:72–79

Srinivasan RS, Bourne DW, Putcha L (1994) Application of physiologically based pharmacokinetic models for assessing drug disposition in space. J Clin Pharmacol 34:692–698

Tan Q, Zhu R, Li H, Wang F, Yan M, Dai L (2012) Simultaneous quantitative determination of paracetamol and its glucuronide conjugate in human plasma and urine by liquid chromatography coupled to electrospray tandem mass spectrometry: application to a clinical pharmacokinetic study. J Chromatogr B Analyt Technol Biomed Life Sci Elsevier BV 893–894:162–7

Tone Y, Kawamata K, Murakami T, Higashi Y, Yata N (1990) Dose-dependent pharmacokinetics and first-pass metabolism of acetaminophen in rats. J Pharmacobiodyn 13:327–335

Tonoli D, Varesio E, Hopfgartner G (2012) Quantification of acetaminophen and two of its metabolites in human plasma by ultra-high performance liquid chromatography–low and high resolution tandem mass spectrometry. J Chromatogr B Analyt Technol Biomed Life Sci Elsevier BV 904:42–50

Vajjah P, Isbister GK, Duffull SB (2012) Introduction to pharmacokinetics in clinical toxicology. Methods Mol Biol 929:289–312

Van der Walt S, Colbert SC, Varoquaux G (2011) The NumPy array: a structure for efficient numerical computation. Comput Sci Eng 13:22–30

Volak LP, Hanley MJ, Masse G, Hazarika S, Harmatz JS, Badmaev V et al (2013) Effect of a herbal extract containing curcumin and piperine on midazolam, flurbiprofen and paracetamol (acetaminophen) pharmacokinetics in healthy volunteers. Br J Clin Pharmacol 75:450–462

Wishart DS, Jewison T, Guo AC, Wilson M, Knox C, Liu Y et al (2013) HMDB 3.0—The Human Metabolome Database in 2013. Nucleic Acids Res 41:D801–D807

Bormann I. DigitizeIt. Available at http://www.digitizeit.de. Accessed 15 Nov 2013

Python Software Foundation. Python Language Reference, version 2.7. Available at http://www.python.org. Accessed 10 Nov 2013

Yin OQ, Tomlinson B, Chow AH, Chow MS (2001) Pharmacokinetics of acetaminophen in Hong Kong Chinese subjects. Int J Pharm 222:305–308

Zhu T, Ding L, Guo X, Yang L, Wen A (2007) Simultaneous determination of tramadol and acetaminophen in human plasma by LC–ESI–MS. Chromatographia 66:171–178